THE JOURNAL OF PHYSICAL CHEMISTRY Letters

Letter

pubs.acs.org/JPCL

High Photoluminescence Efficiency and Optically Pumped Lasing in Solution-Processed Mixed Halide Perovskite Semiconductors

Felix Deschler,[†,§] Michael Price,[†,§] Sandeep Pathak,[†,‡] Lina E. Klintberg,[†] David-Dominik Jarausch,[†] Ruben Higler,[†] Sven Hüttner,[†] Tomas Leijtens,[‡] Samuel D. Stranks,[‡] Henry J. Snaith,*[,‡] Mete Atatüre,[†] Richard T. Phillips,[†] and Richard H. Friend*[,†]

[†]Cavendish Laboratory, JJ Thomson Avenue, Cambridge CB3 0HE, United Kingdom

[‡]Clarendon Laboratory, Parks Road, Oxford OX1 3PU, United Kingdom

Supporting Information

ABSTRACT: The study of the photophysical properties of organic−metallic lead halide perovskites, which demonstrate excellent photovoltaic performance in devices with electron- and hole-accepting layers, helps to understand their charge photogeneration and recombination mechanism and unravels their potential for other optoelectronic applications. We report surprisingly high photoluminescence (PL) quantum efficiencies, up to 70%, in these solution-processed crystalline films. We find that photoexcitation in the pristine $CH_3NH_3PbI_{3-x}Cl_x$ perovskite results in free charge carrier formation within 1 ps and that these free charge carriers undergo bimolecular recombination on time scales of 10s to 100s of ns. To exemplify the high luminescence yield of the $CH_3NH_3PbI_{3-x}Cl_x$ perovskite, we construct and demonstrate the operation of an optically pumped vertical cavity laser comprising a layer of perovskite between a dielectric mirror and evaporated gold top mirrors. These long carrier lifetimes together with exceptionally high luminescence yield are unprecedented in such simply prepared inorganic semiconductors, and we note that these properties are ideally suited for photovoltaic diode operation.

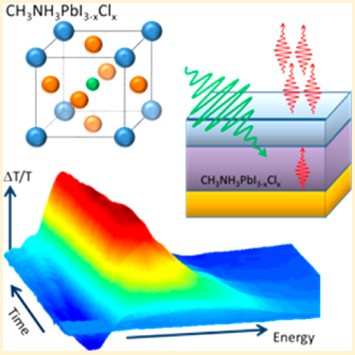

SECTION: Energy Conversion and Storage; Energy and Charge Transport

Organo−lead mixed halide perovskite-based solar cells have shown a breakthrough in power conversion efficiency.[1] Solution-processed devices with power conversion efficiencies of 10−12%[2−6] were reported in 2012 and have more recently exceeded 15% in devices processed by evaporation[7] and sequential deposition.[8] There is evidence from optical studies[9,10] that the diffusion range for the photoexcitations can be substantial, up to 1 μm, and this allows efficient light harvesting across the thickness of the perovskite layer (typically 400 nm). Nevertheless, it has not been clear whether the mobile species is a neutral exciton or free charge, nor is the origin of the high open-circuit voltages clear. As was shown by Lee et al.,[6] the mixed halide perovskite is capable of both electron and hole charge conduction, consistent with the excellent performance of evaporated planar heterojunction structures reported by Liu et al.[7] It was also demonstrated by Burschka et al.[8] that the triiodide perovskite is an efficient sensitizer and can even operate as a hole conductor, sustaining reasonable efficiencies without a hole-acceptor layer.[11] Two-dimensional layer structures with PbI_x layers separated by organic ligands have been extensively investigated by Mitzi et al. and show luminescent properties with excitonic character.[12−16] However, the perovskites used in the present study are three-dimensional semiconductors. A fundamental question is whether the photoexcitation in the perovskite remains as a bound exciton and is later ionized at the electron- and/or hole-accepting heterojunctions (either distributed or planar) or whether charge generation occurs in the pristine perovskite material. In order to address this and also to study the long-time recombination/luminescent processes, we carried out transient photoluminescence (PL) and transient absorption (TA) measurements on spin-coated perovskite films spin-cast onto glass substrates and also of working devices comprising mixed halide perovskite on a compact titanium dioxide electron-accepting electrode with a hole-acceptor layer formed by spin-coating the hole transporter 2,20,7,70-tetrakis(*N*,*N*-di-*p*-methoxyphenylamine)9,90-spirobifluorene (spiro-MeO-TAD).

For sample preparation, methylamine (CH_3NH_2) solution (33 wt %) in absolute ethanol was reacted with hydroiodic acid (HI, 57 wt %) in water with excess CH_3NH_2 under nitrogen atmosphere in ethanol at room temperature. Typical quantities were 24 mL of CH_3NH_2, 10 mL of HI, and 100 mL of ethanol. Crystallization of methylammonium iodide (CH_3NH_3I) was achieved using a rotary evaporator; a white-colored powder was formed, indicating successful crystallization. CH_3NH_3I and lead(II) chloride ($PbCl_2$) were dissolved in anhydrous *N*,*N*-dimethylformamide at a 3:1 molar ratio of CH_3NH_3I to $PbCl_2$

Received: March 14, 2014
Accepted: March 24, 2014
Published: March 24, 2014

   dx.doi.org/10.1021/jz5005285 | *J. Phys. Chem. Lett.* 2014, 5, 1421−1426

to produce a mixed halide perovskite precursor solution. Thin film samples were prepared by spin-coating followed by annealing on a hot plate at 100 °C for 60 min (full details are given in the Supporting Information (SI)).

PL from these materials is emitted in a relatively narrow band centered at 1.6 eV, just below the absorption edge, as shown in Figure S1 (SI). Figure 1a shows the photoluminescence quantum efficiency (PLQE) as a function of excitation fluence for a thin perovskite film on glass.

The PLQE is relatively low at low fluences (<25 mW/cm^2) but rises rapidly above 50% (by 100 mW/cm^2) and reaches a maximum value of 70% at high excitation densities. This is remarkably high and indicates few nonradiative decay pathways. We consider the lower PLQE at low excitation fluence to be due to the presence of defects through which nonradiative decay can occur. Radiative recombination becomes dominant over recombination at high fluences after the defects are filled. The rise in the PLQE toward higher fluences suggests an excitation-density-dependent radiative recombination. We note that comparable PL efficiencies are rarely achieved in untreated inorganic or hybrid materials; thus, nanocrystalline II–VI semiconductors show PL efficiencies of below 15% without special core–shell features, and bulk systems used in solar cells such as copper indium gallium selenide show lower efficiencies.[17−19] It is therefore extremely unusual to find such high PL efficiency, and we consider that this points to a high semiconducting quality and overall low defect density of the spincoated perovskite materials.

We studied the recombination behavior of the photoexcitations in films and solar cells with TA and transient PL spectroscopy on nanosecond time scales to track the excitation density and recombination rate, respectively. Working solar cells based on $CH_3NH_3PbI_{3-x}Cl_x$ perovskites were fabricated with the structure as shown in the inset in Figure S2 (SI). The cells were composed of a thin compact TiO_2 layer (50 nm) deposited on an FTO covered glass substrate followed by a thin (300 nm) mesoporous Al_2O_3 layer onto which the $CH_3NH_3PbI_{3-x}Cl_x$ was deposited by spin-coating.[3,20] This structure was capped with a spiro-MeOTAD layer acting as the hole acceptor and gold electrodes for charge extraction. Before taking TA measurements (details of the laser setup are given in the SI), the power conversion efficiencies of the solar cells were measured in a solar simulator under AM1.5 conditions, yielding values around ∼10% (Figure S3, SI). All measurements were performed at <10 μJ/cm^2, which falls within the linear excitation fluence regime, as verified by a linear response of the TA signal (at zero delay time) and external quantum efficiency (EQE) of the devices up to fluences of 50 μJ/cm^2. At times beyond 1 ps, the TA response shows a ground-state bleaching (GSB) response peaked at 1.65 eV that is spectrally unchanged out to times beyond 200 ns, as shown in Figure S2 (SI). For comparison, Figure S1 (SI) shows the linear absorption and PL spectrum. Any spectral signature due to the spiro-MeOTAD is concealed by the strong perovskite signal, and we consider that the GSB feature at 1.65 eV can be used to track the photoexcitation density as a function of time. We also measured the transient PL of working devices under open-circuit conditions and also of thin films. PL excitation was performed at 2.3 eV with fluences in the range of 2–10 μJ/cm^2. The PL (see Figure S1, SI) showed no detectable spectral evolution with time. At high fluences, we observed a blue shift of the steady-state PL spectrum, by about 50 meV, and a broadening toward higher energies, which indicates state filling

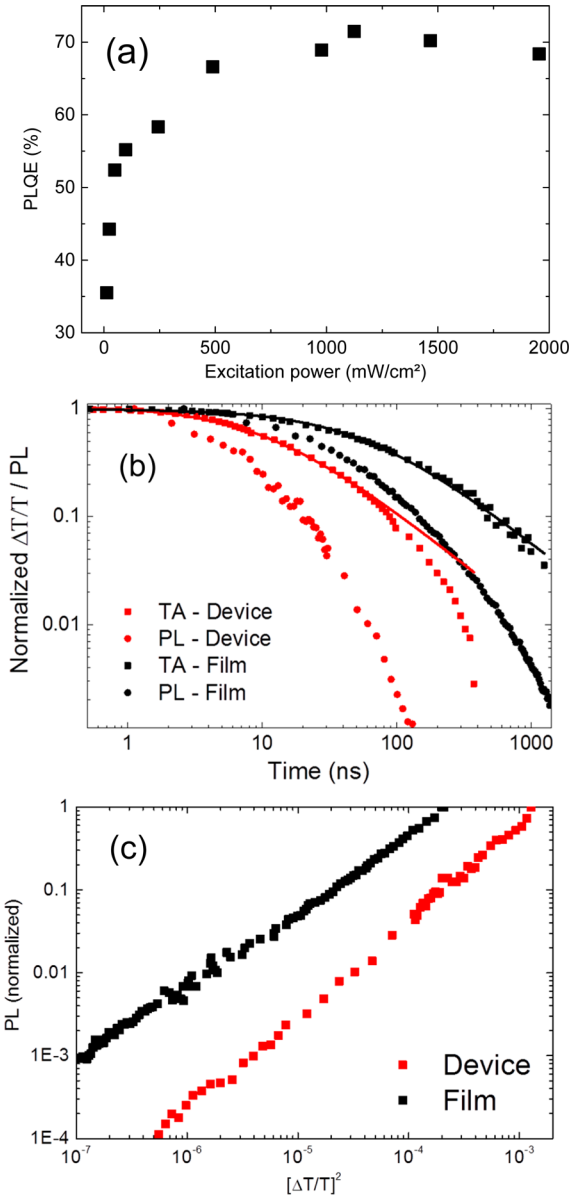

Figure 1. (a) PLQE of $CH_3NH_3PbI_{3-x}Cl_x$ films on spectrosil, annealed in air and capped with a thin PMMA layer. Excitation was performed with a cw laser at 2.33 eV. The integrated PL intensity was taken from 1.77 to 1.46 eV, measured in a Labsphere integrating sphere. The increase in PLQE with excitation fluence indicates a competition between bimolecular recombination and monomolecular, trap-assisted charge recombination. The high values shown here demonstrate that at higher fluences, the dominant mechanism of recombination is radiative. (b) Plot of the normalized PL intensity (integrated from 1.71 to 1.57 eV) and the TA signal versus time for a working device and film samples. Excitation for PL decays of films and devices was performed with a pulsed laser at 2.3 eV and fluence of ∼2 μJ/cm^2. The pulse length was 100 fs and 400 ps for devices and films, respectively. For TA measurements, the device was held at open circuit in a nitrogen-filled holder and was photoexcited at 2.33 eV (10 μJ/cm^2, pulse length 400 ps). The excitation fluence for films was 2 μJ/cm^2. (c) Plot of the normalized PL intensity (integrated from 1.71 to 1.57 eV) versus the square of the TA signal for the samples shown in (b).

of the band structure and emission from higher-lying states[21] (Figure S4, SI). We calculated the expected shift in the PL spectrum from the photoexcitation density ($\rho_{exc} \approx 10^{20}$/cm^3),

dx.doi.org/10.1021/jz5005285 | J. Phys. Chem. Lett. 2014, 5, 1421−1426

the crystal unit size volume[6] ($V \approx 10^{-21}$ cm^3), and the density of states[22] ($g \approx 5$/eV). We found a calculated shift of ~20 meV, which is consistent with the observed shift of ~50 meV and in agreement with previous observations of radiative free carrier recombination in III–V semiconductors.[21]

Figure 1b shows the comparison between the normalized decays of the GSB feature at 1.65 eV and the spectrally integrated PL centered at 1.6 eV.

We find a faster decay of the PL than of the TA. We note that the PL decay reported at low fluences[9,10] is approximately monoexponential (see also Figure S5, SI), but at the higher fluences used here, comparable to those for the TA and only slightly above solar illumination conditions, neither the PL nor the TA can be described by such a monomolecular exponential decay. The solid lines in Figure 1b are fits of the TA decays to a simple bimolecular decay response

$$f(t) = \frac{1}{a + b \cdot t}$$

The film shows the slower decay and is well modeled by this bimolecular rate out to 1 μs. The device shows faster decays that are modeled by this bimolecular rate only at early times. The solid lines in Figure 1b are fits for bimolecular rates of 7.4 $\times$ 10^{-11} (film) and 7.3 $\times$ 10^{-11} cm^3 s^{-1} (device). This value is very close to bimolecular rate constants determined from terahertz measurements of the loss of mobile charge carriers,[23] confirming that the observed PL arises predominantly from charge recombination for films. We note as a comment that films prepared fully under nitrogen conditions show faster kinetics due to intrinsic effects that are reduced when the sample is prepared in ambient conditions (Figure S6, SI).

Figure 1c shows the data of Figure 1b plotted as the normalized PL kinetics versus the square of the absolute GSB kinetics (with time as the implicit variable).

The PL is proportional to the square of the TA for all samples measured, indicating that the PL emission rate is proportional to the square of the excitation density or the product of the electron and hole concentrations (equal for uncontacted films). It is interesting to note that this relationship is observed for films as well as devices that show very different absolute decay rates (see Figure 1b) and different PL strengths. This indicates that, besides charge extraction, mixed halide perovskites show few other nonradiative decay channels in photovoltaic devices, a prerequisite for efficient photovoltaic performance.[24] These results indicate that luminescence in organo–lead mixed halide perovskites $CH_3NH_3PbI_{3-x}Cl_x$ results from bimolecular free carrier electron–hole recombination and highlight the surprisingly high semiconducting quality of these spin-coated and disordered materials.

The evolution of charge generation following photoexcitation is explored in Figure 2a, which shows the TA spectra of perovskite films on glass, excited at 2.33 eV with ultrashort (30 fs) broad-band laser pulses.

Three main spectral features are seen. First, there is a large positive feature that we consider to be GSB that narrows and persists (centered at 1.65 eV at 3 ps), noting that the position of this feature coincides with the absorption edge of pristine $CH_3NH_3PbI_{3-x}Cl_x$ films. We measure a large oscillator strength (~10^{-17} cm^2) for the GSB and consider that it may arise from phase space filling . There is some evidence for a contribution on the low-energy edge from stimulated emission and for a contribution to the signal at higher energies from a change in

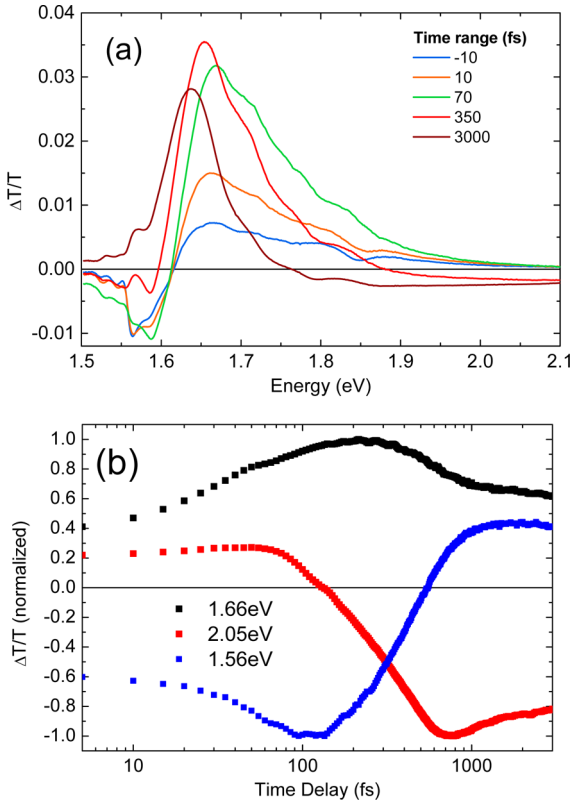

Figure 2. (a) Ultrafast TA spectra of $CH_3NH_3PbI_{3-x}Cl_x$ films on glass at varying delay times up to 3 ps after photoexcitation. Excitation is performed with broad-band laser pulses centered at 2.25 eV with a fwhm of 0.4 eV, pulse length of ~30 fs, and fluence of 1 μJ/cm^2. The spectra show a broad increased transmission centered at 1.7 eV, which gradually red shifts, and a photoinduced absorption (PIA) at higher energies above the band gap. An additional narrow negative feature is observed below the band gap at 1.56 eV, consistent with the electroabsorption spectrum. (b) TA kinetics of $CH_3NH_3PbI_{3-x}Cl_x$ taken at 1.56, 1.66, and 2.05 eV. Signals represent sub-band-gap negative feature, photoinduced transmission peak, and above-band-gap PIA, respectively, from (a). The sub-band-gap negative feature increases on ultrafast time scales (~50 fs) and turns into an increased transmission within 1 ps. A concomitant increase in the above-band-gap PIA is observed. The induced transmission peaks 100 fs after the sub-band-gap PIA and also shows an initial decay up to 1 ps after which the signal persists.

refractive index. Second, a broad, negative (PIA) feature extends toward higher energies (from 1.8 to 2.4 eV), and third, there is a sharper PIA peak at energies (1.56 eV) just below the GSB feature. This last feature decays with a time constant of 400 fs and converts to an increased transmission by 3 ps. We note that the early time spectra are similar to the directly measured electroabsorption spectrum (Figure S7, SI), which is caused by a red shift of the band edge. This red shift can arise through either a band gap renormalization mechanism[25] or an electroabsorption/Stark effect due to correlated charge pair dipoles setting up a strong local electric field within the material.[26] We note that this signal is only short-lived while the other features persist on longer time scales, and its relative intensity (with respect to the bleach at 1.65 eV) increases with decreasing fluence (Figure S8, SI). We consider the sub-band-gap PIA to be a signature for the presence of correlated charge pairs. Similar early time phenomena are observed in III–V systems, and whether or not these can be described as excitonic

dx.doi.org/10.1021/jz5005285 | J. Phys. Chem. Lett. 2014, 5, 1421–1426

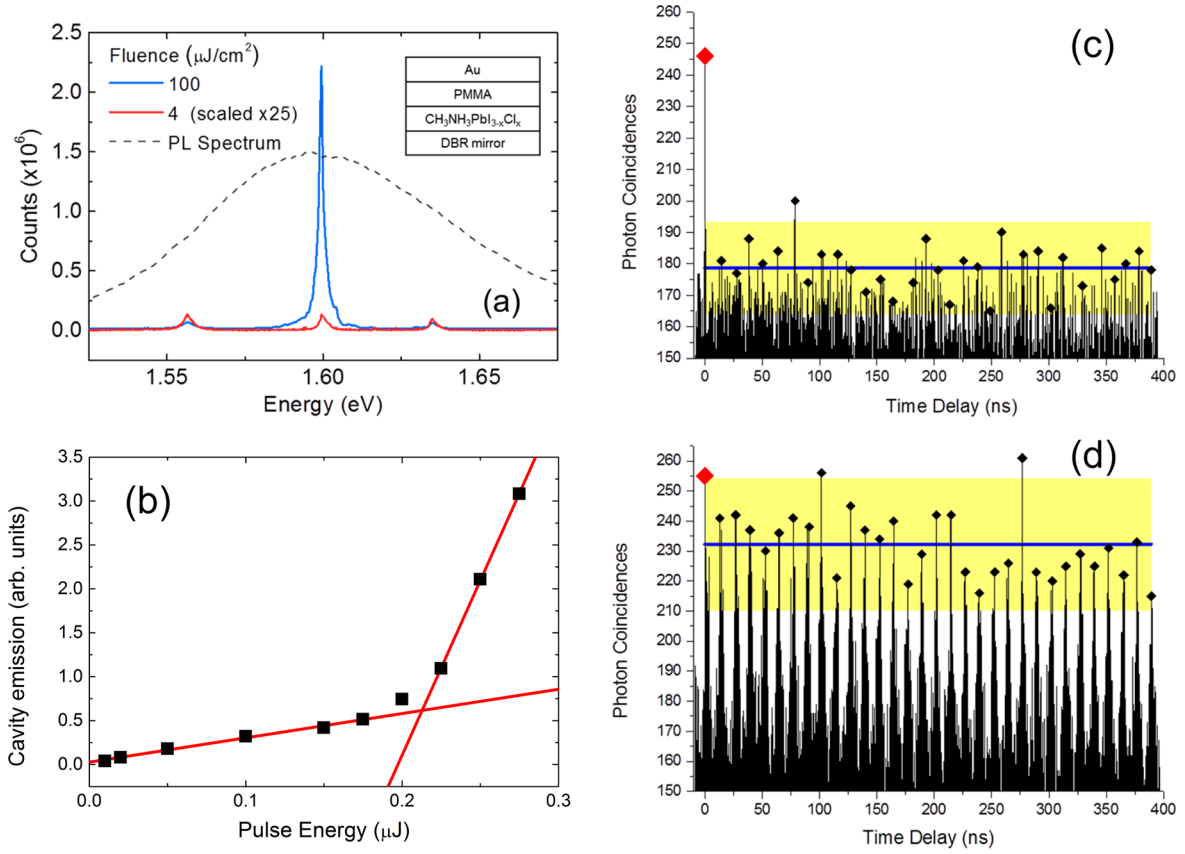

Figure 3. (a) Emission spectrum of a vertical microcavity with the structure as shown in the inset using a perovskite film as the gain medium. The thickness of the perovskite layer was around 500 nm, and it was around 1 μm for the PMMA layer. Excitation was performed with a pulsed laser (400 ps) at 2.33 eV and fluences as stated. At low fluences, three modes are resonant in the cavity with a mode spacing of ~9.5 THz. At sufficiently high fluences, the mode at 1.6 eV is amplified. (b) Correlation between the intensity of the 1.6 eV mode and the pump laser energy showing a lasing threshold at around 0.2 μJ/pulse. (c,d) Intensity correlation measurements of the cavity emission under excitation with 2.33 eV pulses (pulse width of 68 ps, repetition rate of 80 MHz) selectively probing the lasing mode. The positions for zero time delay (red diamond) and the following laser pulses (black diamonds) are indicated. The blue line gives the average peak height, excluding the peak at zero time delay. The yellow area shows the 4σ range. At low fluences (c) a pronounced correlation at zero time delay is found, which indicates photon bunching. At fluences above the lasing threshold (d) the photon bunching effect vanishes, indicating lasing.

populations is actively debated.[27,28] Figure 2b shows the kinetic traces of the main features.

The rise in the broad PIA signal (2.05 eV) is correlated with the decay of the PIA feature at 1.56 eV, and on that same time scale, there is an enhancement in the GSB at 1.65 eV. The response then remains constant after 900 fs, out to times as long as microseconds[9] (Figure S1, SI). The early time spectrum is consistent with the presence of correlated charge pairs, and the observed loss of this signal within a subpicosecond is similar to the time scale of phonon-driven ionization observed in III−V systems.[25] We therefore assign the later time spectrum to that of free charges, which are formed within 1 ps after photoexcitation. This assignment is further supported by the correlation between the kinetics of this feature at longer times and current extraction transients measured in devices (Figure S9, SI).

As a test of the high photophysical quality of the $CH_3NH_3PbI_{3-x}Cl_x$ perovskite semiconductors, we have constructed a vertical cavity optical structure in which a perovskite film is sandwiched between a gold mirror and a standard dielectric stack mirror[29] with a reflectance band from 1.77 eV (see the SI for details on fabrication and measurement). Laser excitation at 2.33 eV with 0.4 ns duration pulses reveals the presence of cavity modes spaced by about 9.5 THz, as shown in Figure 3a.

Above a threshold of 0.2 μJ/pulse, we observe an order of magnitude increase in the slope of the output curve (Figure 3b), line narrowing (Figure S10, SI), and the intensity being transferred to the mode closest to the PL emission peak.

At high fluences, we also observe amplified spontaneous emission (ASE) in thin films (Figure S11, SI), with a significantly broader spectral width compared to the cavity modes. The faster cavity ring down time of the lasing mode compared to the side bands, of order 5 ns, can be seen in Figure S12. Pulsed intensity correlation measurements (Figure 3c and S13) show photon bunching at zero time delay for low excitation densities below the lasing threshold, which is consistent with amplified spontaneous emission. In contrast, similar measurements under high excitation densities (Figure 3d) show a strong suppression of photon bunching, which manifests the high coherence of the emission and therefore lasing. In comparison with previous reports in two-dimensional perovskite systems,[30] we observe lasing at room temperature and do not find a pronounced shift in the PL spectrum compared to low fluences, which rules out previously observed biexcitonic effects.

dx.doi.org/10.1021/jz5005285 | J. Phys. Chem. Lett. 2014, 5, 1421−1426

In summary, we find a very unusual set of characteristics for the mixed halide perovskite $CH_3NH_3PbI_{3-x}Cl_x$ that indicate surprisingly clean semiconducting behavior and give excellent PV performance. Free charges are formed within 1 ps of photoexcitation at room temperature and are long-lived, with a bimolecular decay that gives rise to remarkably efficient PL, particularly at high excitation densities. This indicates that multiple electron−hole collisions can occur within the sample without nonradiative decay. This is a necessary criterion for photovoltaic operation close to the Shockley−Queisser limit,[24] indicating significant future scope for these perovskite solar cells to reach the very highest solar power conversion efficiencies. The high room-temperature PLQE also reveals the potential to use this class of three-dimensional perovskite semiconductors in light-emitting devices because they provide easy injection and transport of both electrons and holes, together with very high luminescence efficiency. These are the properties required for LEDs and injection lasers.

■ ASSOCIATED CONTENT

Supporting Information

Additional figures, including steady-state absorption and PL spectra, TA spectra of photovoltaic devices, current−voltage characteristics of the photovoltaic devices, fluence-dependent PL spectra and kinetics, EA spectra, fluence-dependent TA of films, line-narrowing of the cavity emission, and details of sample fabrication, laser setup, and lasing measurements. This material is available free of charge via the Internet at http://pubs.acs.org.

■ AUTHOR INFORMATION

Corresponding Authors

*E-mail: rhf10@cam.ac.uk (R.H.F.).
*E-mail: h.snaith1@physics.ox.ac.uk (H.J.S.).

Author Contributions

§F.D. and M.P. contributed equally.

Notes

The authors declare no competing financial interest.

■ ACKNOWLEDGMENTS

We thank Dr. Cheng Li and Dr. Dan Credgington for assistance with and helpful discussions on the EA measurements. We thank the Engineering and Physical Sciences Research Council, and the Winton Programme (Cambridge) for the Physics of Sustainability for funding. M.P. wants to thank the Cambridge Commonwealth Trust and the Rutherford Foundation of New Zealand for funding.

■ REFERENCES

(1) Snaith, H. J. Perovskites: The Emergence of a New Era for Low-Cost, High-Efficiency Solar Cells. *J. Phys. Chem. Lett.* **2013**, *4*, 3623−3630.

(2) Abrusci, A.; Stranks, S. D.; Docampo, P.; Yip, H.-L.; Jen, A. K. Y.; Snaith, H. J. High-Performance Perovskite−Polymer Hybrid Solar Cells via Electronic Coupling with Fullerene Monolayers. *Nano Lett.* **2013**, *13*, 3124−3128.

(3) Ball, J. M.; Lee, M. M.; Hey, A.; Snaith, H. J. Low-Temperature Processed Meso-Superstructured to Thin-Film Perovskite Solar Cells. *Energy Environ. Sci.* **2013**, *6*, 1739−1743.

(4) Heo, J. H.; Im, S. H.; Noh, J. H.; Mandal, T. N.; Lim, C.-S.; Chang, J. A.; Lee, Y. H.; Kim, H.-j.; Sarkar, A.; Nazeeruddin, Md. K.; et al. Efficient Inorganic−Organic Hybrid Heterojunction Solar Cells Containing Perovskite Compound and Polymeric Hole Conductors. *Nat. Photonics* **2013**, *7*, 486−491.

(5) Kim, H. S.; Lee, C. R.; Im, J. H.; Lee, K. B.; Moehl, T.; Marchioro, A.; Moon, S. J.; Humphry-Baker, R.; Yum, J. H.; Moser, J. E.; et al. Lead Iodide Perovskite Sensitized All-Solid-State Submicron Thin Film Mesoscopic Solar Cell with Efficiency Exceeding 9%. *Sci. Rep.* **2012**, *2*, 591−598.

(6) Lee, M. M.; Teuscher, J.; Miyasaka, T.; Murakami, T. N.; Snaith, H. J. Efficient Hybrid Solar Cells Based on Meso-Superstructured Organometal Halide Perovskites. *Science* **2012**, *338*, 643−647.

(7) Liu, M.; Johnston, M. B.; Snaith, H. J. Efficient Planar Heterojunction Perovskite Solar Cells by Vapour Deposition. *Nature* **2013**, *501*, 395−398.

(8) Burschka, J.; Pellet, N.; Moon, S.-J.; Humphry-Baker, R.; Gao, P.; Nazeeruddin, Md. K.; Grätzel, M. Sequential Deposition as a Route to High-Performance Perovskite-Sensitized Solar Cells. *Nature* **2013**, *499*, 316−319.

(9) Stranks, S. D.; Eperon, G. E.; Grancini, G.; Menelaou, C.; Alcocer, M. J. P.; Leijtens, T.; Herz, L. M.; Petrozza, A.; Snaith, H. J. Electron−Hole Diffusion Lengths Exceeding 1 Micrometer in an Organometal Trihalide Perovskite Absorber. *Science* **2013**, *342*, 341−344.

(10) Xing, G.; Mathews, N.; Sun, S.; Lim, S. S.; Lam, Y. M.; Grätzel, M.; Mhaisalkar, S.; Sum, T. C. Long-Range Balanced Electron- and Hole-Transport Lengths in Organic−Inorganic $CH_3NH_3PBI_3$. *Science* **2013**, *342*, 344−347.

(11) Etgar, L.; Gao, P.; Xue, Z.; Peng, Q.; Chandiran, A. K.; Liu, B.; Nazeeruddin, Md. K.; Grätzel, M. Mesoscopic $CH_3NH_3PBI_3/TiO_2$ Heterojunction Solar Cells. *J. Am. Chem. Soc.* **2012**, *134*, 17396−17399.

(12) Era, M.; Morimoto, S.; Tsutsui, T.; Saito, S. Organic−Inorganic Heterostructure Electroluminescent Device Using a Layered Perovskite Semiconductor $(C_6H_5C_2H_4NH_3)_2PBI_4$. *Appl. Phys. Lett.* **1994**, *65*, 676−678.

(13) Kitazawa, N.; Watanabe, Y.; Nakamura, Y. Optical Properties of $CH_3NH_3PBX_3$ (X = Halogen) and Their Mixed-Halide Crystals. *J. Mater. Sci.* **2002**, *37*, 3585−3587.

(14) Ishihara, T. Optical Properties of PBI-Based Perovskite Structures. *J. Lumin.* **1994**, *60*−*61*, 269−274.

(15) Mitzi, D. B. Synthesis, Structure, and Properties of Organic-Inorganic Perovskites and Related Materials. In *Progress in Inorganic Chemistry*; Karlin, K. D., Ed.; John Wiley & Sons, Inc.: New York, 2007; pp 1−121.

(16) Mitzi, D. B.; Wang, S.; Feild, C. A.; Chess, C. A.; Guloy, A. M. Conducting Layered Organic−Inorganic Halides Containing ⟨110⟩-Oriented Perovskite Sheets. *Science* **1995**, *267*, 1473−1476.

(17) Talapin, D. V.; Rogach, A. L.; Shevchenko, E. V.; Kornowski, A.; Haase, M.; Weller, H. Dynamic Distribution of Growth Rates within the Ensembles of Colloidal II−VI and III−V Semiconductor Nanocrystals as a Factor Governing Their Photoluminescence Efficiency. *J. Am. Chem. Soc.* **2002**, *124*, 5782−5790.

(18) Dabbousi, B. O.; Rodriguez-Viejo, J.; Mikulec, F. V.; Heine, J. R.; Mattoussi, H.; Ober, R.; Jensen, K. F.; Bawendi, M. G. (CdSe)ZnS Core−Shell Quantum Dots: Synthesis and Characterization of a Size Series of Highly Luminescent Nanocrystallites. *J. Phys. Chem. B* **1997**, *101*, 9463−9475.

(19) Bothe, K.; Bauer, G. H.; Unold, T. Spatially Resolved Photoluminescence Measurements on $Cu(In,Ga)Se_2$ Thin Films. *Thin Solid Films* **2002**, *403*, 453−456.

(20) Eperon, G. E.; Burlakov, V. M.; Docampo, P.; Goriely, A.; Snaith, H. J. Morphological Control for High Performance, Solution-Processed Planar Heterojunction Perovskite Solar Cells. *Adv. Funct. Mater.* **2014**, *24*, 151−157.

(21) Kappei, L.; Szczytko, J.; Morier-Genoud, F.; Deveaud, B. Direct Observation of the Mott Transition in an Optically Excited Semiconductor Quantum Well. *Phys. Rev. Lett.* **2005**, *94*, 147403.

(22) Mosconi, E.; Amat, A.; Nazeeruddin, Md. K.; Gratzel, M.; De Angelis, F. First-Principles Modeling of Mixed Halide Organometal

Perovskites for Photovoltaic Applications. *J. Phys. Chem. C* **2013**, *117*, 13902−13913.
(23) Wehrenfennig, C.; Eperon, G. E.; Johnston, M. B.; Snaith, H. J.; Herz, L. M. High Charge Carrier Mobilities and Lifetimes in Organolead Trihalide Perovskites. *Adv. Mater.* **2014**, *26*, 1584−1589.
(24) Miller, O. D.; Yablonovitch, E.; Kurtz, S. R. Strong Internal and External Luminescence as Solar Cells Approach the Shockley−Queisser Limit. *Photovoltaics, IEEE Journal of* **2012**, *2*, 303−311.
(25) Shank, C. V.; Fork, R. L.; Leheny, R. F.; Shah, J. Dynamics of Photoexcited GaAs Band-Edge Absorption with Subpicosecond Resolution. *Phys. Rev. Lett.* **1979**, *42*, 112−115.
(26) Sebastian, L.; Weiser, G.; Bässler, H. Charge Transfer Transitions in Solid Tetracene and Pentacene Studied by Electroabsorption. *Chem. Phys.* **1981**, *61*, 125−135.
(27) Szczytko, J.; Kappei, L.; Berney, J.; Morier-Genoud, F.; Portella-Oberli, M. T.; Deveaud, B. Determination of the Exciton Formation in Quantum Wells from Time-Resolved Interband Luminescence. *Phys. Rev. Lett.* **2004**, *93*, 137401.
(28) Koch, S. W.; Kira, M.; Khitrova, G.; Gibbs, H. M. Semiconductor Excitons in New Light. *Nat. Mater.* **2006**, *5*, 523−531.
(29) Tessler, N.; Denton, G. J.; Friend, R. H. Lasing from Conjugated-Polymer Microcavities. *Nature* **1996**, *382*, 695−697.
(30) Kondo, T.; Azuma, T.; Yuasa, T.; Ito, R. Biexciton Lasing in the Layered Perovskite-Type Material $(C_6H_{13}NH_3)_2PbI_4$. *Solid State Commun.* **1998**, *105*, 253−255.